Chapter VII

Similarities and differences in motional properties of Staphylococcus aureus exfoliative toxins A and B as revealed by their Molecular dynamics simulation

7.1: Introduction

Staphylococcus aureus can cause a spectrum of exfoliative skin conditions including staphylococcal scalded skin syndrome (SSSS), which can present as a severe and life threatening illness in extremely premature neonates. Kapoor *et al* (2008) describe a case of an extremely premature neonate with SSSS and discuss relevant pathology (Kapoor *et al.,* 2008). The term Staphylococcal scalded skin syndrome (SSSS) is used for a collection of blistering skin diseases induced by the exfoliative (epidermolytic) toxins (ETs) of *Staphylococcus aureus* (Lowney *et al.,* 1967). It primarily affects neonates and young children although adults with underlying diseases are also susceptible. Staphylococcal infections are increases in all age groups worldwide, and show an increasing resistance to conventional antibiotics; despite the availability of a wide range of antibiotics, these infections still carry a significant morbidity and mortality, particularly among adults (Jeyakumari *et al.,* 2009). Because of the relative rarity of the disease and ease of treatment of SSSS has not received as much attention as it deserves by either clinicians or researchers. Furthermore, although the condition was described over a century ago, understanding of it began only when the toxins were discovered (Scopes *et al.,* 1974; Melish & Glasgow 1970; Kapral & Miller 1971). Even now, their mechanism of action is still not certain. However, recent data from computer modeling and crystallography of the toxins has provided us with a clearer and more defined approach to understanding the pathologic processes of the disease (Ladhani *et al.,* 1999). Two serologically distinct forms of exfoliative toxin exist and have been designated as ETA and ETB (Arbuthnott & Billeliffe, 1976; Kondo *et al.,* 1973). The two forms differ in molecular weight, isoelectric point (pI), and amino acid composition (Arbuthnott *et al.,* 1976; Johnson-Winegar & Spero 1983; Wiley & Rogolsky 1977).

X-ray crystallographic structures of ETA and ETB (Cavarelli *et al.,* 1997; Papageorgiou *et al.,* 2000; Vath *et al.,* 1997) suggest that the toxins are members of the trypsin-like serine protease family. Protease activity has not been demonstrated for either toxin in vitro, but both ETA and ETB have intrinsic esterase activity, which is associated with serine proteases (Baile & Redpath 1992). It is likely that both toxins are proteases. In addition to having possible protease activity, both ETA and ETB are reported to be bacterial super antigens (Vath *et al.,* 1997; Marrack & Kappler 1990; Monday *et al.,* 1999; Morlock *et al.,* 1980). The protein ETA contains two domains (I and II) of similar structure, which are built around a six-stranded antiparallel b sheet folded into a β barrel. This architecture is well-known as the serine protease chymotrypsin-like fold, which has been illustrated by several high resolution structures (Perona & Craik 1995; Lesk & Fordham 1996).

ETB consists of two similar domains packed together to form a compact molecule of approximate dimensions 60 × 56 × 36 Å. The core of the molecule contains the "trypsin-like" serine protease fold. Domain 1 is composed of a β-barrel (comprising strands β2–β) surrounded by two short helices (α2 and α3) the C-terminal portion of the molecule that contains two short β-strands (β14 and β15) and a short helix (α5). Domain 2 contains a short amphipathic N-terminal helix (α1) on one side of a six-stranded twisted β-barrel structure (β8–β13) (Papageorgiou *et al.,* 2000). Both ETA and ETB share amino acid identity with staphylococcal V8 protease. This identity includes residues of the V8 protease Ser-His-Asp catalytic triad, a "signature sequence" common to serine proteases. Although this suggests that ETA and ETB are serine proteases, no protease activity has been demonstrated for either toxin to date. However, both ETA and ETB exhibit esterase activities, an activity commonly associated with proteases (Baileyet *et al.,* 1992). In trypsin-like serine proteases, the cleavage of the scissile bond involves formation of a negative charge that is stabilized in

a pocket called the "oxyanion hole," formed by the main-chain atoms (involving the NH groups of Gly193 and Ser195) Surrounding the catalytic serine.

The oxyanion holes of both ETA and ETB are occupied, indicating the crystal structures represent an inactive form of the enzymes. The differing biological activities of the ETs, particularly the lethal and pyrogenic properties of ETB not shared by ETA, likely involve features that are not common between the toxins. The most apparent difference between the ETs is a 14-residue loop extension located before the C-terminal helix in ETB. This large loop is involved in a molecular dimer interface, although the biological relevance of this finding will need to be addressed further. Another potential feature that may be involved in the differing biological properties of the ETs is the small ligand-binding site found in ETA but not ETB. Given the differing structural features on the surface of the ETs, the binding of separate receptors or the same receptor with differing binding modes likely explains the dissimilar functions of the ETs.

Site directed mutagenesis shows that Tyr 157 and Tyr 159 are essential for toxicity. Mutation of any one Tyr reduces the toxicity while double mutation appeared to complete loss of exfoliative activity. Both these residues interact with S1 subsite of Glu182 and Val183. Although both toxins possess similar biological activity, the clustering of tyrosine residue is seen in rETB not in rETA. From the structure based sequence alignment of rETA and rETB in case of rETA tyrosine is not present in aligned position (Papageorgiou *et al.*, 2000)

Elucidating the mechanism of action of the toxins holds exciting prospects for understanding the normal physiology of the skin, targeting drugs to very specific regions of the skin, and developing antitoxins and toxoids that may soon play a vital role in the treatment and prevention of SSSS. (Ladhani *et al.*,1999). In the present work we have done molecular dynamics simulation and principal component analysis of *Staphylococcus aureus*

exfoliative toxins A and B to understand their global and local motional properties which will help to understand it function, mode of action and differences between the toxin A and B.

7.2: Materials and methods

The 2.0A°and 2.8 A° resolution x-ray structure of *Staphylococcus aureus* exfoliative toxins A and B (Protein Data Bank code 1DUA and 1DT2 respectively) (Papageorgiou *et al.,* 2000) were used as starting structures. Each monomer was solvated with SPC water molecules in a cubic box having edge length of 35A°. The simulation was performed using GROMACS (Lindahl *et al.,* 2001). The LINCS algorithm was used to constrain all bond lengths (Hess *et al.,* 1997). A cutoff of 0.9 nm for Lennard-Jones interactions was used and the particle mesh Ewald method (Darden *et al.* 1993; Essmann *et al.,* 1995) was employed to calculate longer-range electrostatic contributions on a grid with 0.12-nm spacing and a cutoff of 1.0 nm. The simulation was conducted at constant temperature (300 K), coupling each component separately to a temperature bath using the Berendsen coupling method (Berenson *et al.,* 1984). The time step was 2 fs, with coordinates stored after every 4 ps. MD simulation was performed for four nano seconds for both the protein 1DUA & 1DT2. Before running simulation, an energy minimization was also performed for both the protein 1DUA & 1DT2 in steepest descent method (converged at 648 and 1050 steps respectively) and this was followed by 1.0ns of simulation imposing positional restraints on the non-H atoms. The positional restraints were then released and 4 ns production run were obtained and analyzed. Analysis programs from GROMACS were used and principal component analysis (PCA) was performed with the MD trajectory.

7.3: Results

The overall structural stability of the protein during the simulation has been monitored using several parameters like RMSD, radius of gyration (Rg), RMSF etc. The time

evolutions of RMSD of the whole protein of Staphylococcus aureus exfoliative toxins A and B during the full simulation time (Fig.1) shows no major difference in case of the structural variation for toxin A and toxin B as measured by RMSD values. RMSD slightly increases upto 3000ps for toxin A and in case of toxin B, simulations become stable after 1000ps.

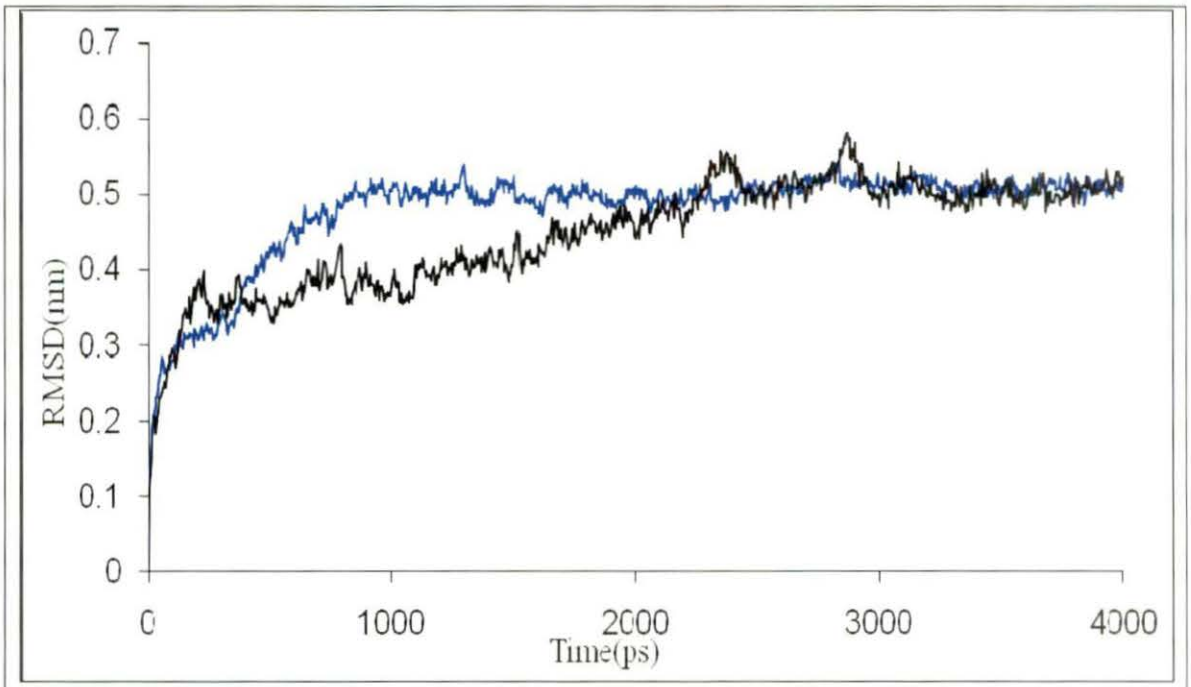

Figure-1: **RMSD:** Root mean square deviations(RMSD) of the protein as a function of time with respect to starting structure during the MD simulations are shown for toxin A i.e., 1DUA(Black) and toxin B i.e.1DT2(blue).

The variation of radius of gyration (Rg) as function of time (Fig. 2) indicates the stability of the simulation i.e. both toxins A and B do not change shape and size during the simulation time. However it is seen that Rg of toxin A remains greater than toxin B during the whole simulation time.

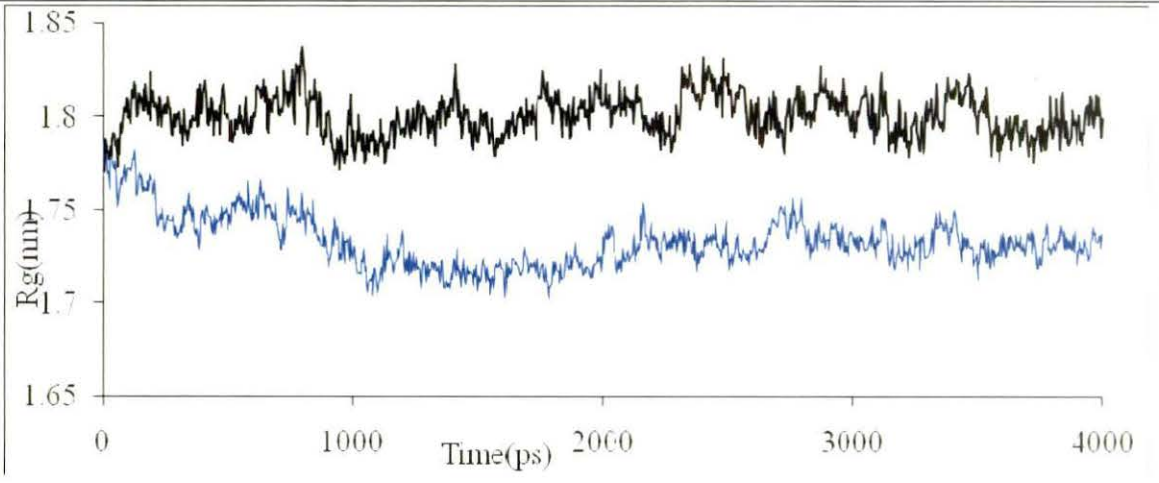

Figure-2: **Radius of gyration**: Radius of gyration (Rg) as a function of time with respect to starting structure during the MD simulations are shown for toxin A i.e., 1DUA (Black) and toxin B i.e.1DT2 (blue).

The flexibility of different segments of the protein is also revealed by looking at the root mean-square fluctuation (RMSF) of each residue from its time-averaged position.

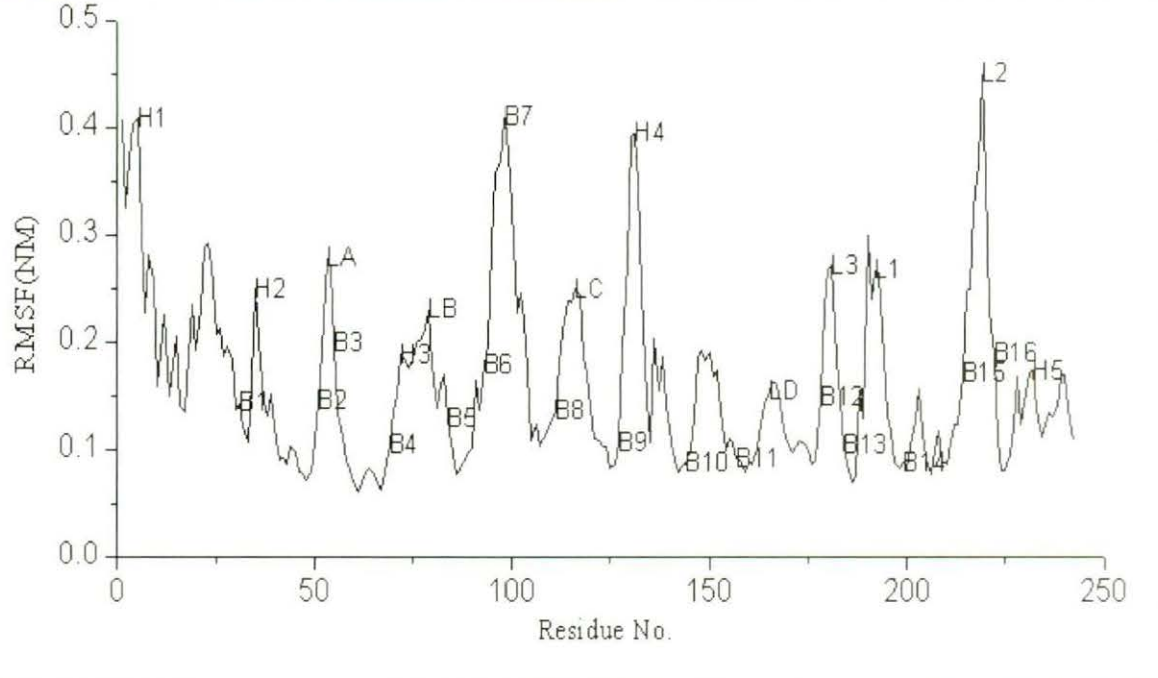

Figure-3a: **Fluctuations:** Root mean squared fluctuations (RMSF) of the Cα atoms during the MD simulations are shown for toxin A (**B**=beta sheet: **H**=helix: **L**=loop)

It is clear from Fig. 3a and 3b that the loop regions have high fluctuations in case of both toxin A and B. Among the secondary structure beta strand has higher fluctuation than alpha helix. Beta sheet 7 has highest fluctuation and sheets 4, 5, 10, 11 have less fluctuation in case of Toxin A whereas in case of toxin B beta sheet 14 has highest fluctuation and sheets 8, 9, 10 have lower fluctuation. Helix4 shows considerable fluctuations for toxin A and Helix2 and Heilix5 shows considerable fluctuations for toxin B.

In order to further explore the nature of the fluctuations, principal component analysis (PCA) is carried out for both the toxins. (Amadei *et al.,* 1993; Garcia 1992; Das & Mukhopadhyay 2007). It is seen that for the toxin A 74.79% fluctuations are captured by first 10 eigenvectors and the first eigenvector corresponds to 35.49% of the total motion and the second 13.81% and third to a further 8.48 %. On the other hand PCA of the toxin B simulation reveals that the first 10 eigenvectors account for 76.61% of the global motion and that the first eigenvector corresponds to 30.42% of the total motion and the second 19.01% and third to a further 10.73 % The first three eigenvectors with largest eigenvalues were selected as the three principal components PC1, PC2, PC3.

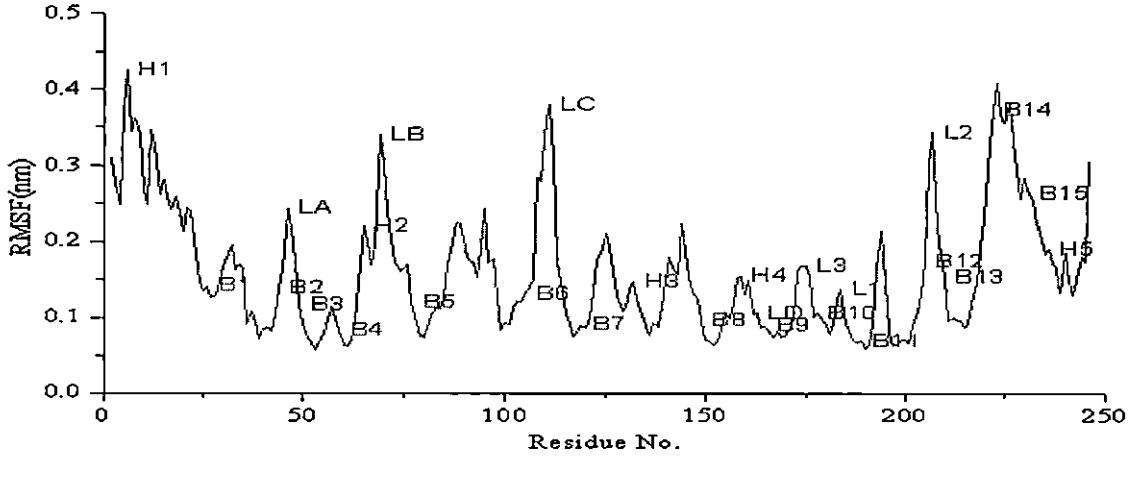

Figure-3b: **Fluctuations:** Root mean squared fluctuations (RMSF) of the Cα atoms during the MD simulations are shown for toxin B (**B**=beta sheet: **H**=helix: **L**=loop)

It is seen that nature of fluctuation of PC1 (Fig. 4a) differs considerably for toxin A and toxin B where as nature fluctuation of PC2 (Fig. 4b) is similar in case of both toxins.

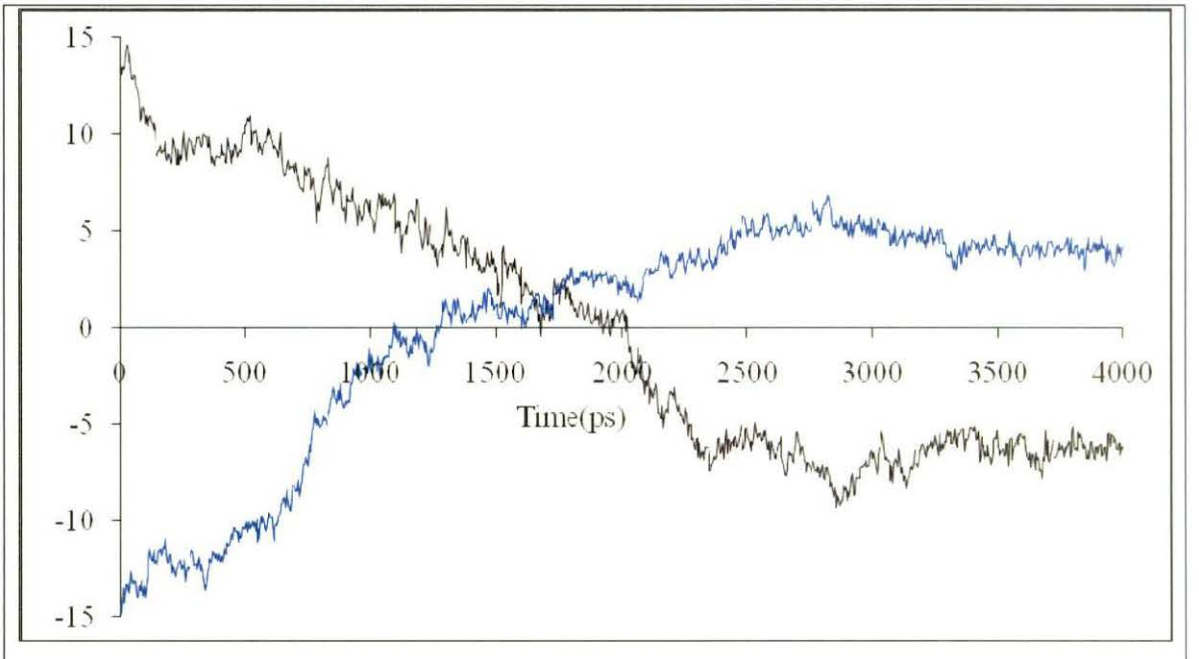

Figure-4a: **Time evolution of PC1**: Variation of principle components 1 with simulation time for toxin A and toxin B[1DUA (Black) and toxin B i.e.1DT2 (blue).

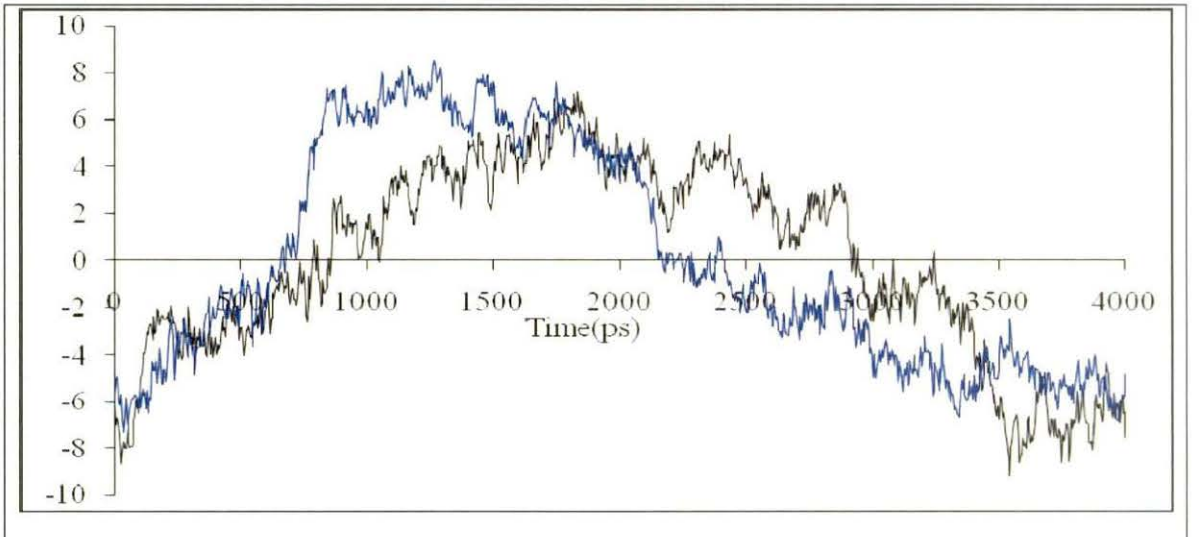

Figure-4b: **Time evolution of PC2**: Variation of principle components 2 with simulation time for toxin B

The RMSF of Cα atoms calculated after projecting trajectories along their respective PC1 and PC2 directions of both the toxins are represented in Fig. 5a and 5b. It is evident for both toxin A and B that fluctuation is highest in the projection on PC1.

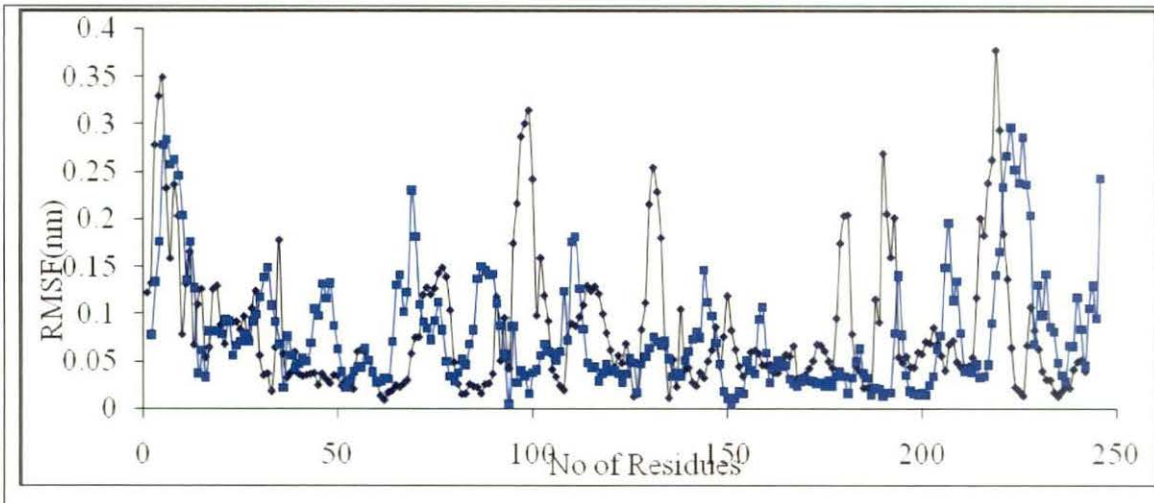

Figure 5a: **Projections on PC1**: The RMSF of Cα atoms calculated after projecting trajectories along their respective PC1 directions [1DUA (Black) and 1DT2 (blue)].

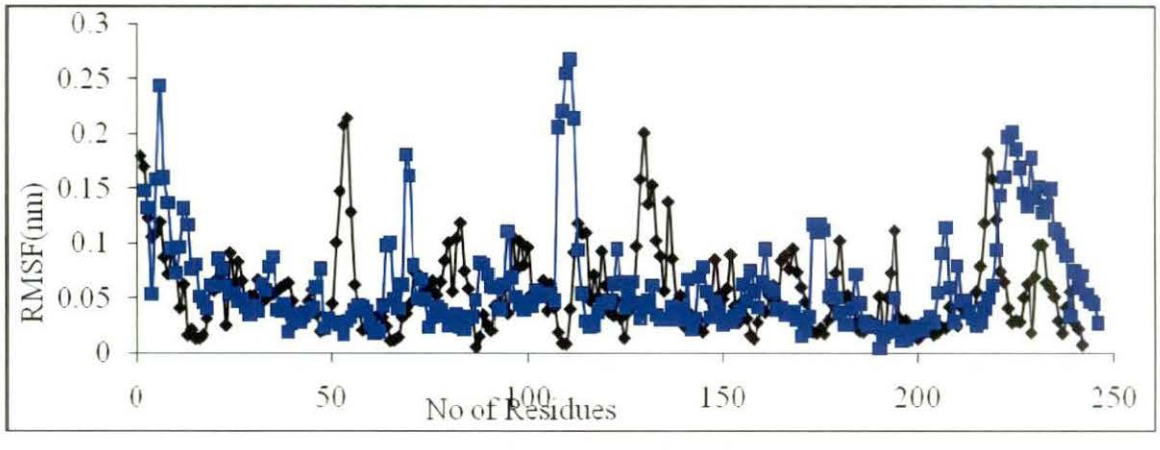

Figure 5b: **Projections on PC2:** The RMSF of Cα atoms calculated after projecting trajectories along their respective PC2 directions [1DUA (Black) and 1DT2 (blue)].

The probability of sampling the phase space determined by first two principal modes during the simulations of toxin A toxin B and presented in Fig. 6.

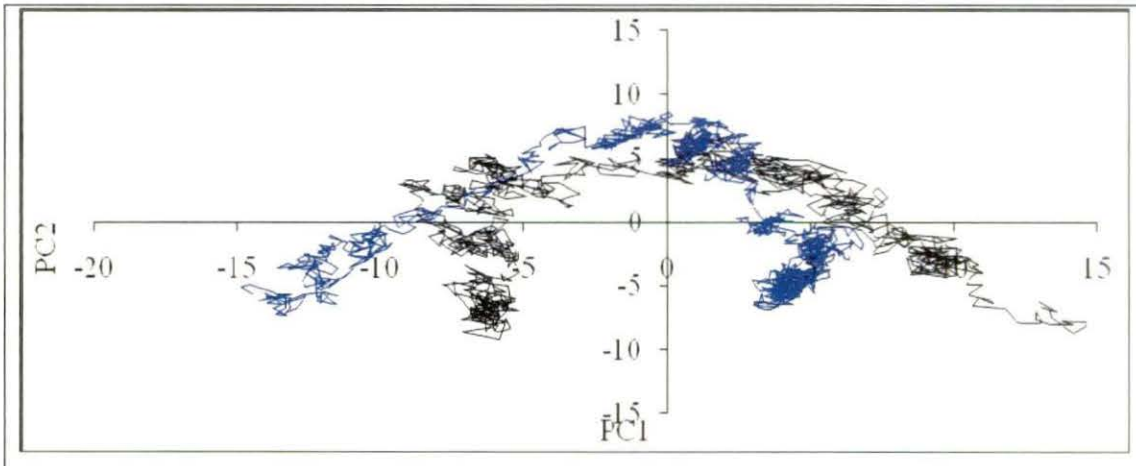

Figure-6: **Conformational Sampling**: The probability of sampling the phase space determined by principal modes 1 and 2 during the simulations of toxin A and toxin B [1DUA (Black) and 1DT2 (blue)].

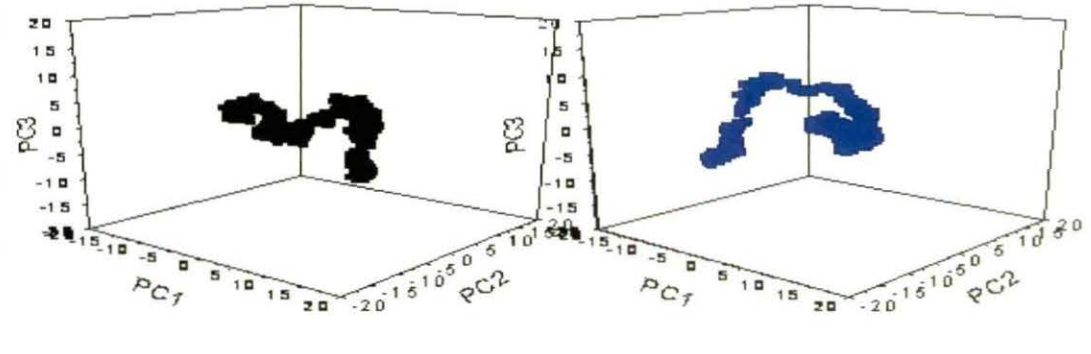

Figure-7: **Space determined PC1, PC2 & PC3 representation**: The probability of accessing regions of the phase space determined PC1, PC2 & PC3 representation for toxin A and B[1DUA (Black) and 1DT2 (blue)].

We further examine the probability of accessing regions of the phase space determined PC1, PC2 & PC3 (Fig. 7) and it is clear that both the toxin show no arrangement in the XY plane and for toxin A almost equally arrange in both the plane YZ and XZ. But molecules of toxin B are more arranged in XZ plane than YZ plane.

In rETA the RMSD values of catalytic residues for Ser195, His72 and Asp120 0.0683, 0.0997, 0.0975 respectively and in rETB, the RMSD values of Ser186, His65, and Asp114 0.038048, 0.1109 and 0.08821. Both Ser195 and Asp120 residue of catalytic triad of rETA are more flexible than in rETB and His65 residue of catalytic triad of rETB is more flexible than in rETA.

In both toxin structures, the primary specificity pocket S1 is formed by residues of domain2 located at the C-terminal end of the molecule in rETA and rETB (in parentheses) are His210 (201), Lys213 (204), Tyr186 (177), and Thr190 (181). In rETA His210 (beta sheet 15), Lys 213(beta sheet 15), Tyr186 (beta sheet 13) and Thr190 (loop1) are important residues for determination the specificity of the substrate and their the RMSD values are 0.0349, 0.073, 0.0273 and 0.0515 respectively and in rETB, the RMSD values of His201 (beta sheet 12), Lys204 (beta sheet 12), Tyr177 (beta sheet 10) and Thr181 (loop1) are 0.031994, 0.074635, 0.028007 and 0.020468. It is clear that only Thr190 (loop1) has high fluctuation in toxin A in comparison to toxin B where the fluctuations of other residues are comparable. Hydrogen bond network is responsible for the overall stability of the protein during simulation although, during whole simulation several hydrogen bonds break and formed.

It is found that the number of hydrogen bonds ranges from 143 to 197 for Toxin B and 141-205 for toxin A. While analyzing the hydrogen bond of binding site it is found only one hydrogen bond remains stable in toxin A throughout the simulation (HB9 formed between carbonyl oxygen of Val119 and the amide nitrogen atoms of Leu121) which belongs to loop C Whereas in case of toxin B three hydrogen bonds remain intact (HB2-, HB4 formed between amide nitrogen of Gly184 and the carbonyl oxygen atoms of Glu182 & the side chain nitrogen atoms of Asn185, HB9 the hydrogen atom of hydroxyl group of Tyr177 and the side chain nitrogen atom of his 201(H9)).HB2 and HB4 form within the Loop1 residues and HB9 forms within beta sheets 10 and 12.

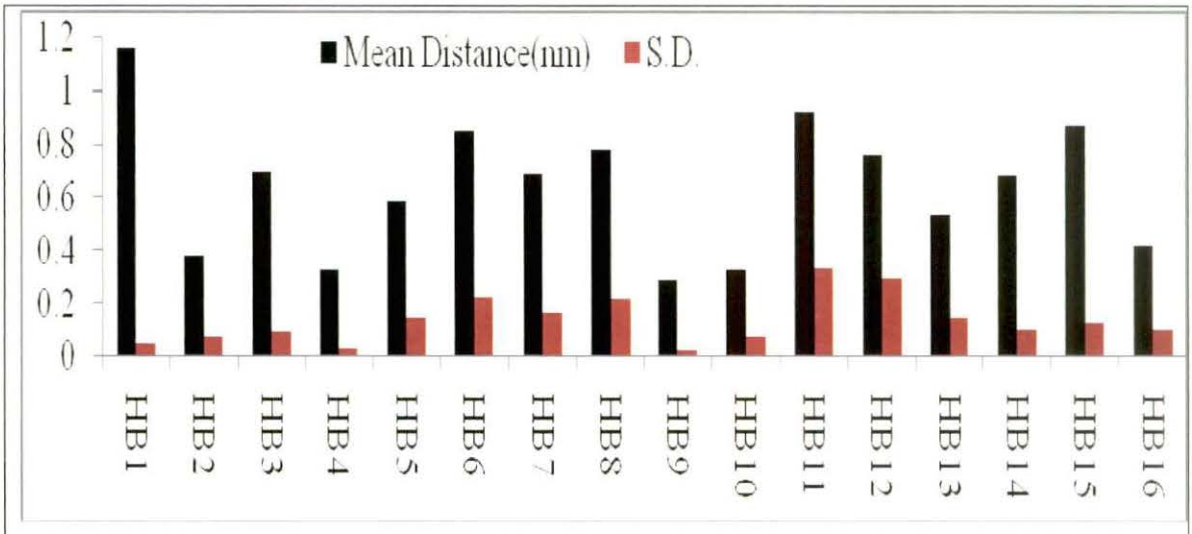

Figure-8a: **Hydrogen bond of toxin A:** Hydrogen bonds within the binding site region of toxin A during the simulation time

HB1: Hydrogen bonds between carbonyl oxygen of Trp14 and the amide nitrogen atom of Tyr18

HB2: Hydrogen bond between side chain oxygen of Tyr18 and the amide nitrogen atoms of Arg71

HB3: Hydrogen bond between the side chain oxygen of Try18 and the amide nitrogen atoms of Thr190

HB4: Hydrogen bond between the carbonyl oxygen of Arg71 and the amide nitrogen atoms of Ala74

HB5: Hydrogen bond between the side chain oxygen of Asp120 and the amide nitrogen atoms of Arg71

HB6: Hydrogen bond between the side chain oxygen of Asp120 and the side chain nitrogen atoms of His72

HB7: Hydrogen bond between the side chain oxygen of Asp120 and the amide nitrogen atoms of His72

HB8: Hydrogen bond between both side chains of Asp120 and Ser211,

HB9: Hydrogen bond between carbonyl oxygen of Val119 and the amide nitrogen atoms of Leu121

HB10: Hydrogen bond between the hydrogen atom of hydroxyl group Tyr186 and the side chain nitrogen atom of His210

HB11: Hydrogen bond between both side chains of Thr190 and Lys213

HB12: Hydrogen bond between the side chain oxygen of Asn194 and the side chain nitrogen atoms of Val191

HB13: Hydrogen bond between the carbonyl oxygen of Val191 and the amide nitrogen atoms of Asn194

HB14: Hydrogen bond between the carbonyl oxygen of Pro192 and the amide nitrogen atoms of Ser195

HB15: Hydrogen bond between the carbonyl oxygen of Pro192 and the side chain of Ser195 (H15),

HB16: Hydrogen bond between the side chain oxygen of Asp164 and the amide nitrogen atoms of Gly193

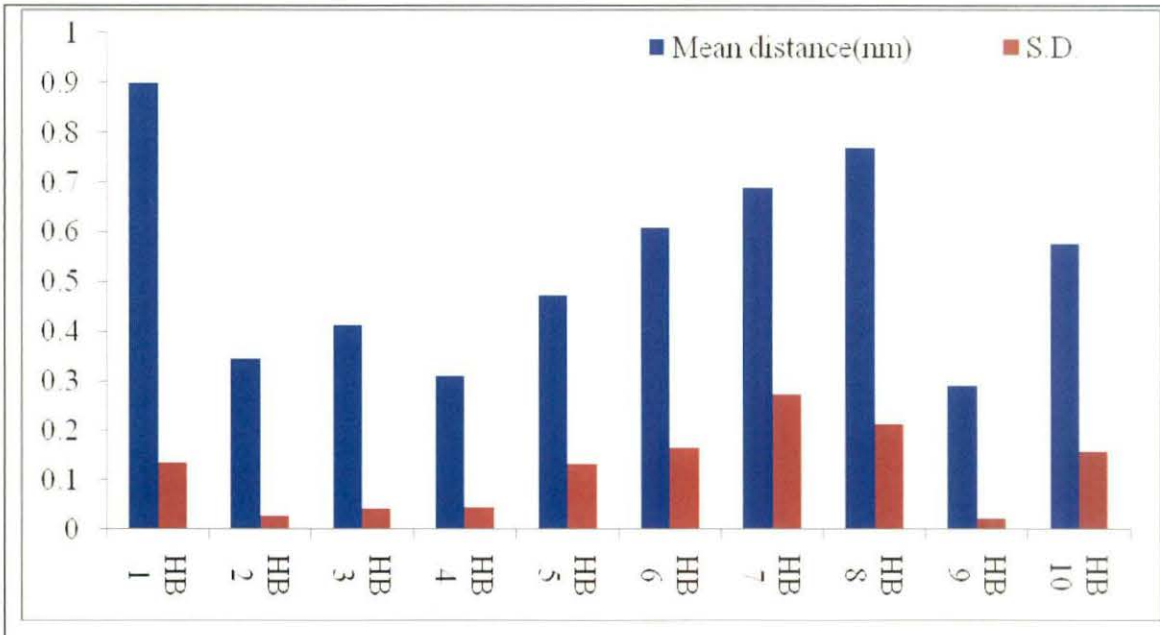

Figure-8b: **Hydrogen bond of toxin B:** Hydrogen bonds within the binding site region of toxin B during the simulation time

HB1: Hydrogen bond between amide nitrogen of Asn158 and the side chain oxygen atoms of Glu182

HB2: Hydrogen bonds formed between amide nitrogen of Gly184 and the carbonyl oxygen atoms of Glu182 (H2)

HB3: Hydrogen bonds between carbonyl oxygen of Glu182 and the amide nitrogen atoms of Asn185 (H3),

HB4: Hydrogen bonds formed between amide nitrogen of Gly184 and the side chain nitrogen atoms of Asn185 (H4),

HB5: Hydrogen bond between the side chain oxygen atom of Glu182 and the hydrogen atom of hydroxyl group Tyr180

HB6: Hydrogen bond between amide nitrogen of Tyr64 and the side chain oxygen atoms of Asp114 (H6)

HB7: Hydrogen bond between the amide nitrogen of His65 and the side chain oxygen atoms of Asp114 (H7),

HB8: side chains of Asp114 and Ser202 (H8),

HB9: Hydrogen bond between the hydrogen atom of hydroxyl group Tyr177 and the side chain nitrogen atom of His201 (H9),

HB10: Hydrogen bond between both side chains of His65 and Ser186,(H10)

There are several hydrogen bonds, which fluctuate during simulation time, some time they cross the limit of hydrogen bond distance (HB2, HB4, HB10, HB16 for toxin A and HB3for

toxin B)(Fig. 8a, 8b). Other hydrogen bonds in binding site region for both the toxins were broken during simulation time.

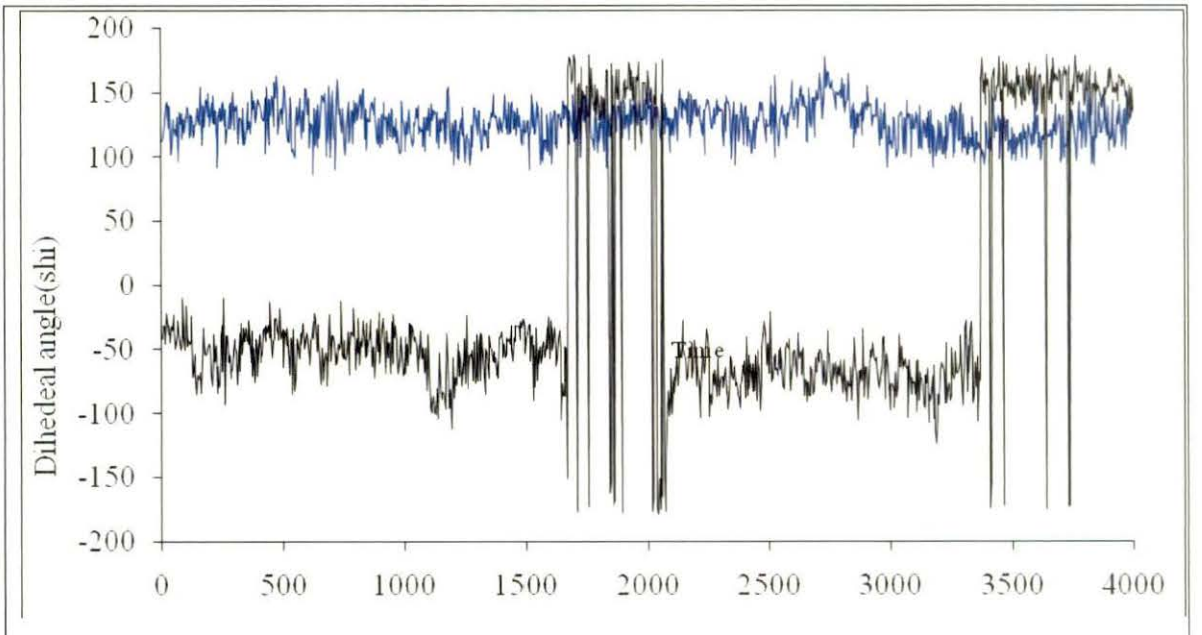

Figure-9: **Dihedral angle of catalytic triad**: Distribution of shi for the Res. Pro192 of toxinA and val183 of toxin B during simulation [1DUA (Black) and 1Dt2 (blue)].

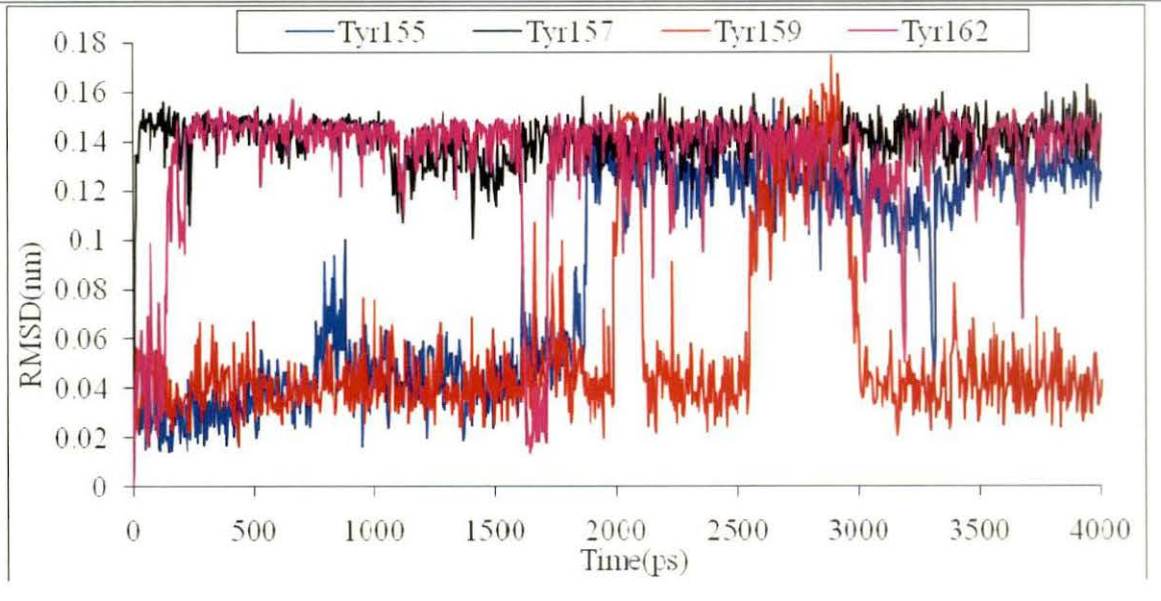

Figure-10: **RMSD of cluster of tyrosine residues:** Time evolution RMSD of cluster of tyrosine residues in rETB (positions 155, 157, 159, and 162)

Time evolution of ψ for the Res. Pro192 of oxyanion hole of toxin A and val183 of toxin B during simulation are shown in Fig. 9. It is seen that Pro192 of toxin A shows a conformational transition where Val183 (corresponding residue from sequence alignment) do not show any conformational transition.

Among the four tyrosine residue it is seen that fluctuation of Tyr162 is lowest and that of Tyr157 and Tyr9 are large indicating their high mobility which enable them to interact with other residues (Fig. 10).

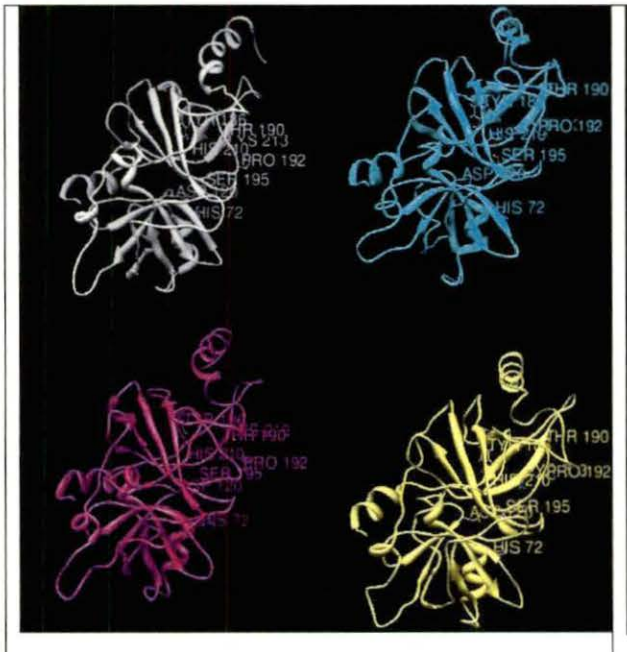

Figure-11a: **Snapshot:** Snapshot of the toxin A (200ps- white 1100ps-pink, 2100ps- green and 3000ps- yellow) are presented in this figure

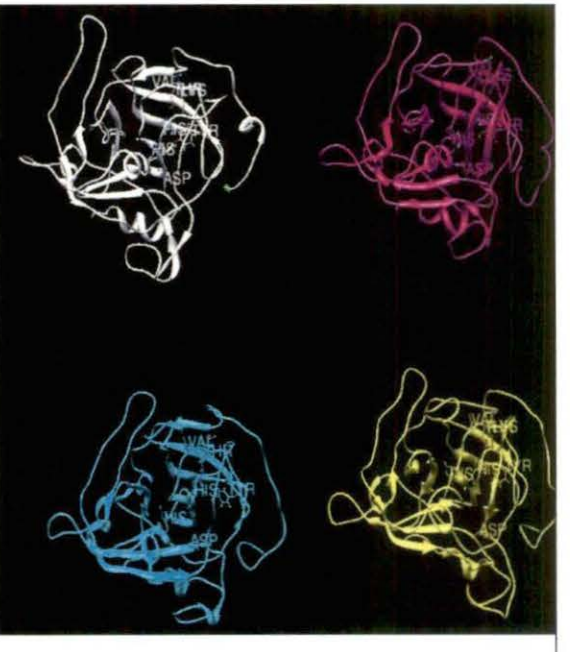

Figure-11b: **Snapshot:** Snapshot of the toxin B (200ps- white 1100ps-pink, 2100ps- green and 3000ps- yellow) are presented in this figure

Snapshot of the toxin are presented in Fig. 11a and 11b where Pro192 (Val183) an important residue of oxyanion hole, catalytic triad residues Ser195 (Ser186), His72 (his65) & Asp120 (Asp114) and the primary specificity pocket S1 residues His210 (His201),

Lys213 (Lys204), Tyr186 (Tyr177) & Thr190 (Thr181) are labeled for rETA and rETB respectively (in parentheses).

The plot of distance of Cα-Cα of interacting residues of S1 subsite and helix 4 of toxin B residues during simulation time (Fig. 12) shows the residue come together during simulation and interact with each other, we tried to find whether any hydrogen bond is formed between these residues, we observed no hydrogen bond is formed. So vanderwaals interaction is responsible for their interaction.

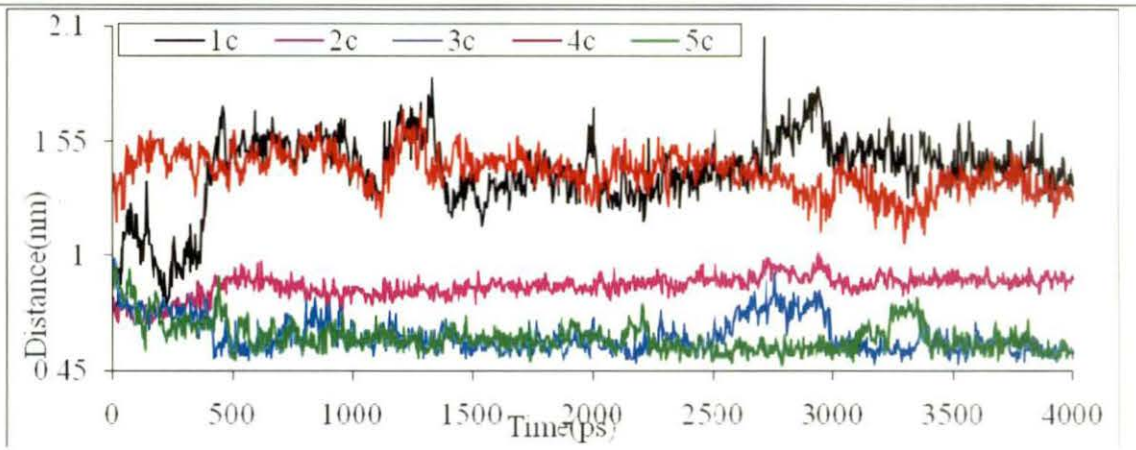

Figure-12: **Cα-Cα distance of interacting residues**: Time evolution Cα-Cα distance of interacting residues of S1 subsite and helix 4 of toxin B

C1: Distance between Cα atoms of residues Pro19 and tyr159

C2: Distance between Cα atoms of residues Glu182 and tyr157

C3: Distance between Cα atoms of residues Val183 and tyr159

C4: Distance between Cα atoms of residues Glu16 and Lys204

C5: Distance between Cα atoms of residues Thr181 and Lys204

7.4: Discussion

Toxin A and B have high degree of sequence and structural similarity. We investigated the motional properties of the toxins in this work. During the dynamics, the structural variations, as measured by the RMSD and the radius of gyration as a function time for both

toxins suggest that the simulations are stable. It is also evident that toxin B is somewhat more rigid than toxin A. From RMSF analysis it is evident that nature of fluctuation for different secondary structures and loop regions are similar in both toxin A and toxin B.

From the RMSF of Cα atoms calculated after projecting trajectories along their respective Principal components (PC1 & PC2) indicate that fluctuation is higher in case of toxin A along both the PC i.e. PC1 & PC2. (Fig. 5a, 5b).

It is clear from the probability of sampling the phase space determined by first two principal modes during the simulations the projection of the dynamics trajectory onto the first two PC that the protein A traverse one conformational space around the origin and another at the right side of the origin and also at the left side of the origin. It is evident from Fig. 6 that conformational freedom is more at the left side of the origin. In rETA Hydrogen bond between carbonyl oxygen of Val119 and the amide nitrogen atoms of Leu121 (H9), was very strong suggesting the loop C is less flexible than toxin B. The hydrogen bonds between carbonyl oxygen of Trp14 and the amide nitrogen atom of Tyr18 (H1) were broken during energy minimization which indicates that the helix1 is much flexible.

In rETB Glu182 Gly184 and Asn185 belong to loop1 The two strong hydrogen bonds were observed in the amide nitrogen of Gly184 and the carbonyl oxygen atoms of Glu182 (H2) carbonyl oxygen of Glu182 and the side chain nitrogen atoms of Asn185 (H4), suggest that that loop1, is less flexible in toxin B than toxin A. The hydrogen atom of hydroxyl group of Tyr177 and the side chain nitrogen atom of His 201(H9) forms another strong hydrogen bond also reveal that beta sheets 10 and 12 are also strong because tyr177 belongs beta sheet 10 and the residue His201 belongs from sheet 12. Overall we can say that loop1 and beta sheets of 10 and 12 are conserved. The hydrogen bond between amide nitrogen of Asn158 and the side chain oxygen atoms of Glu182 (H1) were broken during energy minimization increases the flexibility helix-4 because Asn158 belong helix 4, at the same

time Glu182 of S1 subsite (loop 1) has less flexible because it forms another two strong hydrogen bonds mention above.

In both toxin structures, the primary specificity pocket S1 is formed by residues of domain 2 and in both structures the binding of substrate in the S1 pocket may be stabilized by His210 (201). (Cavarelli et al. 1997) The positioning of Tyr186 (177) helps in optimal orientation of His210 (201) on one side of the pocket. Moreover, Lys213 (204) a residue conserved in both ETs, interacts with the side chain of the glutamate moiety in the S1 pocket. Low RMSD values of those residues support the above facts. In trypsin-like serine proteases, the cleavage of the scissile bond involves formation of a negative charge that is stabilized in a pocket called the "oxyanion hole," formed by the main-chain atoms (involving the NH groups of Gly193 and Ser195 in ETA and Gly184 and ser 186 in ETB) surrounding the catalytic serine (Papageorgiou *et al.,* 2000). In rETA, Pro192 and Gly193 have a unique conformation. In this case negative charge developed by tetrahedral transition state is stabilized by a conformational change of the loop, which needs a rotation of psi of pro192 from helical to strand nature. Residue Pro192 of Toxin A overcomes the energy barrier and folded into another structure, on the other hand Val183 of toxin B ψ value was very stable, remaining throughout our simulation shown in Fig. 9.

It is seen from the plot of psi against simulation, the dihedral is free to rotation without involvement of much energy. During the simulation several times it jumps from -40^0 regions to 180^0 regions.

Thus inactive toxin A becomes active gaining the preferred conformation. From the time evolution of Val 183 the corresponding residue of toxin B, it is seen that the psi of has very less freedom, its value remains close to 140^0 without any major valine183 deviation. It is clear that in case of toxin B this residue is in preferred conformation to show activity. This

observation clearly indicates that pro192 and val183 is key residue towards the activity and why toxin A and toxin B show the difference in initiation of activity.

It is reported that mutation of Tyr157, Tyr159 causes the loss activity of the toxin B (Papageorgiou *et al.,* 2000). High RMSD of these residues is supportive to the fact their interaction S1 subsite residues is energetically favourable. From the plot of distance between Cα-Cα of interacting residues of S1 subsite and helix 4 of toxin B against simulation time it also revealed that these residues are highly mobile and their mobility do not require much energy and any hindrance on their conformational free has immense impact on activity.

7.5: References

Amadei A, Linssen ABM & Berendsen HJC. (1993) Essential dynamics of proteins. *Proteins: Struct. Funct. Genet.* **17**: 412–425.

Arbuthnott JP & Billeliffe B (1976) Qualitative and quantitative methods for detecting staphylococcal epidermolytic toxin. *J. Med. Microbiol.* **9**:191-201.

Bailey CJ & Redpath MB (1992). The esterolytic activity of epidermolytic toxins. *Biochem. J.* **284:**177–180.

Berendsen HJC, Postma JPM, DiNola A & Haak JR. (1984) Molecular dynamics with coupling to an external bath. *J. Chem. Phys.* **81**:3684–3690.

Cavarelli J, Prevost G, Bourguet W, Moulinier L, Chevrier B, Delagoutte B, Bilwes A, Mourey L, Rifai S, Piemont Y & Moras D (1997) The structure of *Staphylococcus aureus* epidermolytic toxin A, an atypic serine protease, at 1.7 A resolution. *Structure* **5:**813–824.

Darden T, York D & Pedersen L (1993) Particle mesh Ewald: An $N\cdot\log(N)$ method for Ewald sums in large systems. *J. Chem. Phys.* **98**:10089–10092.

Das A & Mukhopadhyay C (2007) Application of principal component analysis in protein unfolding: An all-atom molecular dynamics simulation study. *The Journal of Chemical Physics* **127**, 165103-165108.

Essmann U, Perera L, Berkowitz ML, Darden T, Lee H & Pedersen LG (1995) A smooth particle mesh Ewald method. *J. Chem. Phys.* **103**:8577–8593

Garcia AE (1992) Large-amplitude nonlinear motions in proteins. *Phys. Rev. Lett.* **68**:2696–2699.

Hess B, Bekker H, Berendsen HJC & Fraaije JGE (1997) LINCS: A linear constraint solver for molecular simulations. *Journal of Computational Chemistry* **18**:1463-1472.

Jeyakumari D, Gopal R, Eswaran M & MaheshKumar C (2009) The staphylococcal scalded-skin syndrome in a new born. *Journal of Global Infectious Diseases* **1**:45-47.

Johnson-Winegar AD & Spero L (1983) Isoelectric focusing patterns of staphylococcal exfoliative toxin. *Curr. Microbiol.* **8**:311-315.

Kapoor V; Travadi, J & Stephen B (2008) Staphylococcal scalded skin syndrome in an extremely premature neonate: A case report with a brief review of literature. Journal of *Paediatrics & Child Health.* **44:** 374-376

Kapral FA & Miller MM (1971) Product of *Staphylococcus aureus* Responsible for the Scalded-Skin Syndrome. *Infection and Immunity.* **4**: 541-545.

Kondo I, Sakurai S & Sarai Y (1973) Purification of exfoliation produced by *Staphylococcus aureus* of bacteriophage group 2 and its physicochemical properties. *Infect. Immun.* **8**:156-164.

Ladhani S, Joannou CL, Lochrie DP, Evans RW & Poston SM (1999) Clinical, microbial, and biochemical aspects of the exfoliative toxins causing staphylococcal scalded-skin syndrome. *Clin Microbiol Rev.* **12**:224–242.

Lesk AM & Fordham WD (1996) Conservatiuon and variability in the structures of serine proteinases of the chymotrypsin family. *J. Mol. Bio.***258:** 501-537.

Lindahl E, Hess B & van der Spoel D (2001) GROMACS 3.0: a package for molecular simulation and trajectory analysis. *J. Mol. Modeling* **7**:306-317.

Lowney ED, Baublis JV Kreye GM, Harrell ER & McKenzie AR (1967) The scalded-skin syndrome in small children. *Arch. Dermatology.* **95**:359-369.

Marrack P & Kappler J (1990). The staphylococcal enterotoxins and their relatives. *Science.* **248:**750–711.

Melish ME & Glasgow LA (1970) The staphylococcal scalded-skin syndrome. *N. Engl. J. Med.* **282:**1114–1119.

Monday SR, Vath GM, Ferens WA, Deobald C, Rago JV, Gahr PJ, Monie DD, Iandolo JJ, Stephen K. Chapes SK, Davis WC, Ohlendorf DH, Schlievert PM & Bohach GA (1999). Unique superantigen activity of staphylococcal exfoliative toxins. *J. Immunol.* **162:**4550–4559.

Morlock BA, Spero L & Johnson AD (1980). Mitogenic activity of staphylococcal exfoliative toxin. *Infect. Immun.* **30:**381–384.

Papageorgiou AC, Plano LR, Collins CM & Acharya KR (2000). Structural similarities and differences in *Staphylococcus aureus* exfoliative toxins A and B as revealed by their crystal structures. *Protein Sci.* **9: 610-618.**

Perona JJ & Craik CS (1995) structural basis of substrate specificity in the serine proteases. *Protein Sci.* **4 337-360**

Scopes JW, Eykyn S & Phillips I (1974) Staphylococcal infection in the newborn. *The Lancet* **304**:1392.

Vath GM, Earhart CA, Rago JV, Kim MH, Bohach GA, Schlievert PM & Ohlendorf DH (1997). The structure of the superantigen exfoliative toxin A suggests a novel regulation as a serine protease. *Biochemistry.* **36:**1559–1566.

Vath GM, Earhart CA, Monie DD, Iandolo JJ, Schlievert PM & Ohlendorf DH (1999). The crystal structure of exfoliative toxin B: a superantigen with enzymatic activity. *Biochemistry* **38:**10239–10246.

Wiley BB & Rogolsky M (1977) Molecular and serological differentiation of staphylococcal exfoliative toxin synthesized under chromosomal and plasmid control. Infect. *Immun.* **18**:487-494.